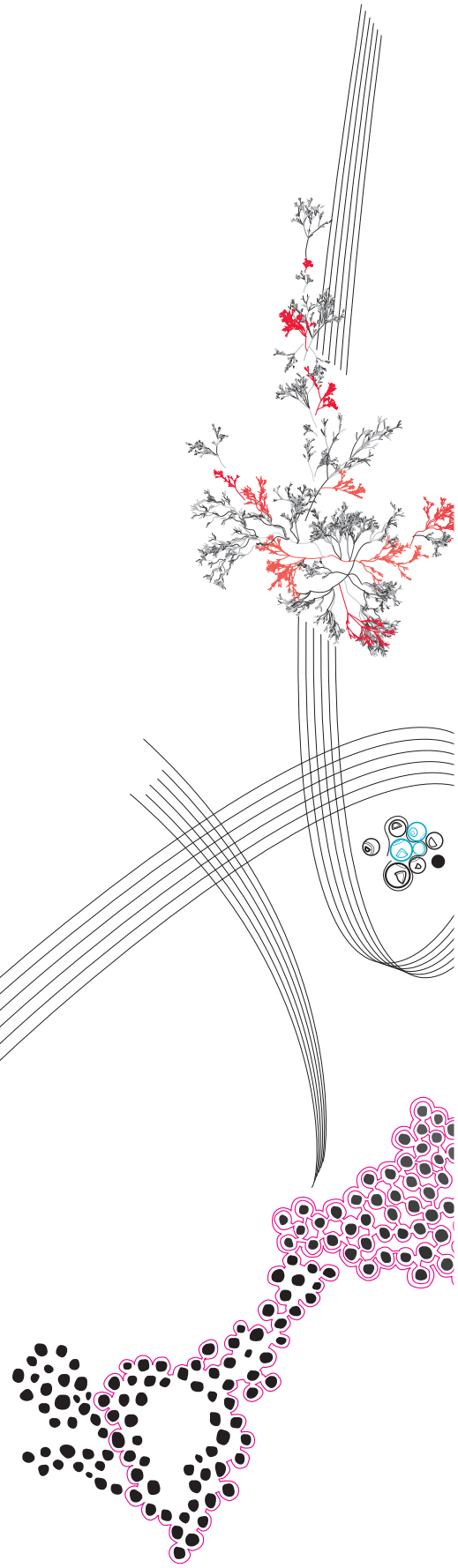

BSc Thesis Applied Mathematics

Investigating the effect of graphene nanofillers on the melting of paraffin-based phase change materials

J. Chris Petri

Supervisors: Prof.Dr.Ir. B.J. Geurts, K.A. Redosado Leon, MSc

June, 2023

Department of Applied Mathematics
Faculty of Electrical Engineering,
Mathematics and Computer Science

UNIVERSITY OF TWENTE.

Preface

This research was part of the Bachelor's assignment that marks an end to the three-year journey that was the BSc Applied Mathematics. I look forward to a new adventure in the MSc programme.

I would like to express my sincere gratitude to Bernard Geurts and Kevin Redosado for their supervision and guidance throughout this study. Your input has positively influenced my research and your feedback greatly contributed to the quality of my work.

Investigating the effect of graphene nanofillers on the melting of paraffin-based phase change materials

J. Chris Petri*

June, 2023

Abstract

Phase change materials have emerged as a critical player in the quest to make energy storage more sustainable and efficient. Due to its properties, paraffin plays a crucial role in this development, despite its low thermal conductivity. To overcome this, graphene nanofillers are introduced to enhance the overall thermal conductivity. This paper presents a means to analyse the effect of graphene nanofillers on the distribution of heat throughout a substance that undergoes a phase transition from solid to liquid. This so-called two-phase Stefan problem involves heat conduction equations for the liquid and solid regions, together with a moving boundary interface. Due to its complexity, it is reformulated using the enthalpy formulation. The one-dimensional two-phase Stefan problem is solved using both an exact solution and numerical approximation. The accuracy of the numerical approximations is validated by comparing them with the exact solutions, providing confidence in the correctness of the results. This validation extends to the two-dimensional numerical solutions. Simulations highlight the enhancement of the performance of phase change materials. It is clear that graphene nanofillers substantially increase the rate of the phase transition process.

Keywords: Phase change problems, Stefan problem, moving boundary interface, enthalpy formulation

*Email: j.c.petri@student.utwente.nl

Table of Contents

1 Introduction

As the world increasingly seeks renewable energy sources with sporadic availability, phase change materials (PCMs) are emerging as a critical player in the energy industry, as they offer unique thermal energy storage capabilities. PCMs are a type of material that undergo a phase change within a convenient temperature range, enabling it to absorb and release thermal energy without having to go to very high temperatures - much energy can be stored as latent heat, thereby leading to compact solutions for the storage of considerable amounts of energy. In particular, paraffin-based PCMs have gained significant attention due to their strong heat storage properties [1]. Due to the organic origin and relatively cheap nature, paraffin is a competitive candidate in the race toward sustainability.

The main disadvantage of paraffin-based phase change materials is the rather low thermal conductivity [2, 3]. This leads to a limited dispersion of heat within the substance, resulting in the need for research to improve the characteristics and thus the performance of PCMs. In this study, we are interested in the addition of nanofillers which have a higher thermal conductivity. The addition of such nanofillers is believed to enhance the performance of PCMs, by increasing the overall thermal conductivity [4, 5, 6]. Specifically, in this study we look at graphene nanofillers. There are different implications of nanofillers that may be considered. In this study, we assume the application of graphene nanofillers will be realised as a mixture between paraffin and graphene, viewed from a macroscopic perspective. That is, we will see any mixture of graphene and paraffin as a homogeneous substance.

Our goal in this research is to develop and analyse a model that closely represents paraffin-based PCMs with graphene as a nanofiller. We will investigate the thermal behaviour of phase transition processes for PCMs with and without nanofillers. In particular, we are interested in the phase transition of a solid to liquid state. The main question we want to answer in this study is:

"What changes does heat transport in paraffin-based phase change materials undergo, when transitioning from a solid to a liquid state, and what is the effect of graphene nanofillers in this process?"

Research on phase change materials has the potential to add a significant contribution to developing renewable and durable energy solutions. This potential positive impact on the environment - known as stewardship - provides a powerful inducement to contribute to the research of the development of phase change materials.

We start this thesis with an introductory chapter to give the reader a general reading of phase change problems. In this section, we introduce the mathematics behind heat equations and phase change problems and derive the mathematical models that will be used, specifically the model that describes the phase interface or moving boundary, which is the interface between two adjacent phases, i.e., between liquid and solid.
Subsequently, we will derive an exact one-dimensional solution in Chapter 3 that will be utilized later in this thesis for validation purposes. Hereafter, we introduce the enthalpy formulation, which is a method to describe the moving boundary problem such that it is more convenient to solve this problem. The numerical methods that are used to approximate such a solution are discussed in Chapter 5, together with the accuracy of these methods. Additionally, an overview of the sequential steps in our simulation process is

provided in this chapter.

We end this study in Chapter 6 with a discussion of the simulation results that are obtained from exact and numerical methods. We will validate the accuracy and correctness of the numerical method, after which we will perform parameter sensitivity analysis to investigate the impact of different thermal properties. Subsequently, we discuss two-dimensional simulations that will give a more complete view of the thermal behaviour of PCMs. Using these simulations, we will answer the aforementioned main question of this study.

2 Fundamentals of phase change problems: An overview and contextual background

In this chapter, we delve into the essential foundations of phase change problems. In Section 2.1, we will explore the physical interpretation and understanding of phase change problems. Subsequently, in Section 2.2, we look into the mathematics surrounding moving boundary problems. Specifically, in Sections 2.2.1 and 2.2.2 we introduce the mathematics that describes the moving boundary problem and derive an equation for its behaviour. We conclude this chapter by making a remark on a non-dimensional moving boundary problem.

In this chapter, we give the reader a first foundation with which an understanding is possible regarding the discussions in subsequent chapters, concerning the analytical and numerical analysis and simulations.

2.1 Physical background

A phase change problem is a physical occurrence where, due to the addition or release of energy, the material changes its state of aggregation which results in a discontinuous change in its thermodynamic properties. The most evident thermodynamic properties that change after a change of phase, are density, thermal conductivity and specific heat capacity. Density refers to the mass of a substance divided by its volume. Due to the expansion of material at higher temperatures, the density has an inverse relation with temperature. Thermal conductivity is a measure of the ability of a material to conduct heat. Due to alterations in its molecular or atomic arrangement, the conductivity of a substance may change after a phase change. Specific heat capacity refers to the amount of energy required to raise a substance one temperature unit. In this study, we consider the temperature unit to be Celsius. We can think of the phase change as an isothermal process. During this process, energy is absorbed or released as heat and contributes to the amount of matter that changes phase. The corresponding heat stored or released is known as latent heat. Due to the absorbing or releasing of the latent heat, the interface that separates two different states moves.

2.2 Mathematical foundation

Before we can model a moving boundary problem, we first need a way to properly describe the heat distribution of more standard systems. In 1878, Joseph Fourier laid the foundation of such heat equations [7]. To get familiar with these equations, we will show the derivation of the heat equation in a one-dimensional rod, which is defined on the finite interval $x \in [a, b]$. We first look at the thermal energy of the system. The thermal energy in a thin cross-section of the one-dimensional rod may be written as $\epsilon(x, t)A\Delta x$, where ϵ

denotes thermal energy density, A the area of the cross-section and Δx the length of the slice [8]. The total thermal energy may accordingly be defined as

Thermal energy

$$\begin{aligned} \epsilon(x,t)A\Delta x &= c_p(x)\rho(x)u(x,t)A\Delta x \\ \epsilon(x,t) &= c_p(x)\rho(x)u(x,t) \end{aligned} \tag{2.1}$$

Here, c is the specific heat, ρ the density and u the heat distribution of the substance.

We assume the one-dimensional rod to be of homogeneous material. This assumption implies that the properties of specific heat capacity, c_p and density, ρ, remain constant throughout the rod. Hence,

$$\epsilon(x,t) = c_p\rho u(x,t) \tag{2.2}$$

Following the first law of thermodynamics, we obtain

$$\frac{d}{dt}\int_a^b \epsilon\, dx = \phi(a,t) - \phi(b,t) + \int_a^b \mathcal{Q}\, dx \tag{2.3}$$

where $\mathcal{Q}$ is defined as a heat source and ϕ denotes the heat flux. Using the Fundamental Theorem of Calculus,

$$f(b) - f(a) = \int_a^b \frac{d}{ds} f(s) ds \tag{2.4}$$

we obtain the equation

$$\int_a^b \left(\frac{\partial \epsilon}{\partial t} + \frac{\partial \phi}{\partial x} - \mathcal{Q} \right) dx = 0 \tag{2.5}$$

As this integral must be zero for all arbitrary points a and b, the integrand must be equal to zero as well. Hence,

$$\frac{\partial \epsilon}{\partial t} = -\frac{\partial \phi}{\partial x} + \mathcal{Q} \tag{2.6}$$

Fourier's law

The heat flux ϕ is related to the gradient of the temperature through

$$\phi = -k\nabla u(x,t) \tag{2.7}$$

Here, k denotes the thermal conductivity of the substance.

Following the definition of thermal energy as described in Equation (2.1) and substituting Fourier's law as described in Equation (2.7) we obtain

$$c\rho\frac{\partial u}{\partial t} = \frac{\partial}{\partial x}\left(k\frac{\partial u}{\partial x} \right) + \mathcal{Q} \tag{2.8}$$

For convenience, we let

$$\alpha = \frac{k}{c\rho} \tag{2.9}$$

where α is known as the thermal diffusivity. This yields the one-dimensional heat equation

General heat equation

$$\frac{\partial u}{\partial t}(x,t) = \alpha \frac{\partial^2 u}{\partial x^2}(x,t) + \mathcal{Q}(x,t) \tag{2.10}$$

If there is no external heat source, this equation becomes

$$\frac{\partial u}{\partial t}(x,t) = \alpha \frac{\partial^2 u}{\partial x^2}(x,t) \tag{2.11}$$

Note that in this derivation, we assumed a high level of differentiability. In this study, we assume that all heat equations are sufficiently smooth to satisfy the differentiability condition. The heat equations for multi-dimensional systems can also be determined. An example is given in Equation (2.12), where a three-dimensional system is denoted.

$$\frac{\partial u}{\partial t} = \alpha \left(\frac{\partial^2 u}{\partial x^2} + \frac{\partial^2 u}{\partial y^2} + \frac{\partial^2 u}{\partial z^2} \right) \tag{2.12}$$

In this section, we have explored the mathematical foundation of heat equations. Although derived for one-dimensional systems, a general equation for three-dimensional systems is also introduced. With the physical and mathematical interpretation of this problem, we continue with the mathematical formulation of moving boundary problems.

2.2.1 The Stefan problem

Phase change problems where phase transitions such as solidification or melting occur, are called Stefan problems, named after physicist Josef Stefan. Depending on the number of phases that occur, they are often called N-phase Stefan problems. In Figure 1, two phases can be observed in the illustration. Hence, we call this a two-phase Stefan problem. In this section we will discuss such problems. Let us look at the mathematical implication of phase-change problems for the melting of solids. Consider a semi-infinite one-dimensional solid defined on $x > 0$ having phase-change temperature, i.e. melting temperature T_m. Furthermore, we assume that the initial temperature of the solid region has a uniform temperature T_S such that $T_S < T_m$. At time $t = 0$, the temperature at boundary $x = 0$ is raised to T_L such that $T_L > T_m$, which is maintained for all $t > 0$.

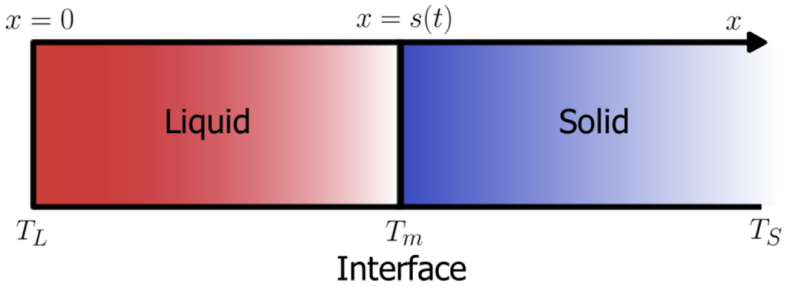

FIGURE 1: An illustration of the two-phase Stefan problem where $T_L > T_m > T_S$

We recognise two distinct regions. The first region is said to be liquid and the second region is solid. Both regions are separated by a moving phase-change interface. An illustration of this Stefan problem is given in Figure 1. Due to the boundary temperature $T_L > T_m > T_S$, the phase-change interface moves towards the positive x-direction. The two sections with

different phases follow the general heat equation as described in Equation (2.11) and are denoted in Equations (2.13a-2.13b). Additionally, the corresponding boundary conditions are introduced.

Heat equations of the Stefan problem

$$\frac{\partial u_L(x,t)}{\partial t} = \alpha_L \frac{\partial^2 u_L(x,t)}{\partial x^2} \quad \text{for } 0 < x < s(t),\ t > 0 \tag{2.13a}$$

$$\frac{\partial u_S(x,t)}{\partial t} = \alpha_S \frac{\partial^2 u_S(x,t)}{\partial x^2} \quad \text{for } x > s(t),\ t > 0 \tag{2.13b}$$

Boundary conditions

$$u_L(0,t) = T_L$$
$$u_S(x \to \infty, t) \to T_S$$

Initial value

$$u_S(x,0) = T_S$$

Here, $u(x,t)$ describes the temperature distribution and α the thermal diffusivity. The subscript denotes the correspondence to the liquid (L) or solid (S) region. We assume that the liquid and solid phases can be described by separate constant values for α_L and α_S. Furthermore, $s(t)$ describes the location of the moving phase-change interface to which we turn next.

2.2.2 The Stefan condition

To obtain a solution for the preceding Stefan problem, the location of the interface has to be evaluated together with the solution to the corresponding heat equations. This is also called the Stefan condition. It may be seen in Equations (2.13a-2.13b) that this condition serves as an interface condition at $x = s(t)$.
We assume that at the interface, the temperature is continuous between phases. Hence,

$$\lim_{x \to s(t)^-} u_L(x,t) = \lim_{x \to s(t)^+} u_S(x,t) = T_m \quad \forall\, t > 0 \tag{2.14}$$

where T_m denotes the phase-change temperature.
We consider the cross-section of the interface to have an area A at some time $t = t_0$. At some later time $t_1 = t_0 + \Delta t$ for sufficiently small Δt, the interface has shifted to a position $s(t_1) > s(t_0)$. During the time interval $[t_0, t_1]$, a volumetric section of $A \cdot (s(t_1) - s(t_0))$ has been melted. This yields a total absorbed quantity of heat of

$$Q = mL = A\rho\,(s(t_1) - s(t_0)) \cdot L \tag{2.15}$$

where m denotes a unit of mass, which is calculated by the volumetric section of the melted area, multiplied by its density ρ. L denotes the specific latent heat. Assuming there are no additional sinks or sources, we take advantage of the law of conservation energy. We

again utilize Fourier's law, as depicted in Equation (2.7).

$$\begin{aligned} Q &= \int_{t_0}^{t_1} \int_A \left[\phi_L \cdot \hat{i} + \phi_S \cdot \left(-\hat{i} \right) \right] dA \, d\tau \\ &= \int_{t_0}^{t_1} \int_A \left[-k_L \nabla u_L(s(\tau), \tau) \cdot \hat{i} - k_S \nabla u_S(s(\tau), \tau) \cdot \left(-\hat{i} \right) \right] dA \, d\tau \\ &= A \int_{t_0}^{t_1} \left[k_S \frac{\partial u_S}{\partial x}(s(\tau), \tau) - k_L \frac{\partial u_L}{\partial x}(s(\tau), \tau) \right] d\tau \end{aligned} \tag{2.16}$$

Here, $\hat{i}$ denotes the unit vector in the x-direction. Recall that A denotes the area of the cross-section of the interface, k the thermal conductivity and u the temperature distribution. Recall that the subscripts L and S denote the liquid and solid phase of the substance, respectively. Now, equating Equation (2.15) and (2.16), we obtain

$$A\rho \left(s(t_1) - s(t_0) \right) \cdot L = A \int_{t_0}^{t_1} \left[k_S \frac{\partial u_S}{\partial x}(s(\tau), \tau) - k_L \frac{\partial u_L}{\partial x}(s(\tau), \tau) \right] d\tau \tag{2.17}$$

Using the Fundamental Theorem of Calculus, we obtain

Stefan condition

$$L\rho \frac{\partial s}{\partial t} = k_S \left. \frac{\partial u_S}{\partial x}(x,t) \right|_{x=s(t)} - k_L \left. \frac{\partial u_L}{\partial x}(x,t) \right|_{x=s(t)} \quad \text{for } t > 0 \tag{2.18}$$

Boundary condition

$$u_L(s(t), t) = u_S(s(t), t) = T_m$$

We refer to Equation (2.18) as the Stefan condition, which was desired to complete the formulation of the problem [9, 10]. The Stefan condition states that the rate of change of thermal energy in the material is determined by the difference in heat fluxes at the phase interface.

2.2.3 Nondimensionalization

The one-dimensional system may now be nondimensionalized to obtain a mathematically more convenient formulation. Nondimensinalization is a common technique to simplify equations and reduce to the essential parameters. To nondimensionalize the Stefan condition as found in Equation (2.18), we introduce some changes [10]. The following nondimensionalized parameters are defined:

$$\eta = \frac{x}{b}, \quad \tau = \frac{\alpha_L t}{b^2}, \quad \theta(\eta, \tau) = \frac{u_i(x,t) - T_m}{T_m - T_L} \quad \text{and} \quad \delta(\tau) = \frac{s(t)}{b}, \quad \text{for } i \in \{L, S\}$$

where b is a reference or characteristic length. Additionally, we introduce β, which is defined as the inverse of the so-called Stefan number, defined as

$$\text{Ste} = \beta^{-1} = \frac{c_p \left(T_m - T_L \right)}{L} = \frac{c_p \Delta T}{L} \tag{2.19}$$

where c_p denotes the specific heat, L the latent heat and ΔT the difference in temperature between a reference and melting temperature. The reference temperature refers to the

temperature of the energy source. The Stefan number emphasizes the crucial role played by the ratio between sensible heat relative to latent heat. Previous derivation yields the dimensionless interface equation

$$\beta \frac{d\delta(\tau)}{d\tau} = \frac{k_S}{k_L} \frac{\partial \theta_S}{\partial \eta} - \frac{\partial \theta_L}{\partial \eta} \tag{2.20}$$

Here, we can see the prominent presence of the Stefan number. The Stefan number is crucial for solving the moving boundary problem. In the next chapter, we will discuss a solution for the Stefan condition and see the importance of the Stefan number.

3 An analytical solution to the moving boundary problem

In this section, an exact solution of the Stefan problem will be derived. Recall from Section 2.2.1 that these problems are called N-phase Stefan problems, dependent on how many phases occur. Note that if $N = 1$, we have a general heat conduction problem. For this study, we are interested in two-phase Stefan problems, as we assume both the liquid and solid part of the substance to have a different temperature than the phase-change temperature. Recall that this problem is illustrated in Figure 1.

3.1 Neumann's solution

Consider the phase-change problem as defined in Section 2.2.1.

Heat equations of the Stefan problem

$$\frac{\partial u_L(x,t)}{\partial t} = \alpha_L \frac{\partial^2 u_L(x,t)}{\partial x^2} \quad \text{for } 0 < x < s(t),\ t > 0 \tag{3.1a}$$

$$\frac{\partial u_S(x,t)}{\partial t} = \alpha_S \frac{\partial^2 u_S(x,t)}{\partial x^2} \quad \text{for } x > s(t),\ t > 0 \tag{3.1b}$$

$$L\rho \frac{\partial s}{\partial t} = k_S \left.\frac{\partial u_S}{\partial x}(x,t)\right|_{x=s(t)} - k_L \left.\frac{\partial u_L}{\partial x}(x,t)\right|_{x=s(t)} \quad \text{for } t > 0 \tag{3.1c}$$

Boundary conditions

$$u_L(0,t) = T_L$$
$$u_S(x \to \infty, t) \to T_S$$
$$u_L\left(s(t),t\right) = u_S\left(s(t),t\right) = T_m$$

Initial value

$$u_S(x,0) = T_S$$

We want to find a solution for the location of the phase interface ($s(t)$), as for the temperature distribution in the liquid and the solid region. To obtain an exact solution for the interface, we first have to solve the Stefan problem for $u_L(x,t)$ and $u_S(x,t)$. To obtain this solution, we use the similarity solution [8]. We introduce the similarity variable

$$\xi = \frac{x}{\sqrt{t}}, \quad \text{for } t > 0 \tag{3.2}$$

such that $u(x,t) = f(x/\sqrt{t}) = f(\xi)$. Substituting $f(\xi)$ into a temporal first and spatial second order partial derivative yields

$$\frac{\partial u}{\partial t} = \frac{1}{2}\frac{x}{\sqrt{t^3}}\frac{\partial f}{\partial \xi} \tag{3.3}$$

$$\frac{\partial^2 u}{\partial x^2} = \frac{1}{t}\frac{\partial^2 f}{\partial \xi^2} \tag{3.4}$$

Substituting these equations into Equation (3.1a), we obtain the following first-order linear ordinary differential equation:

$$-\frac{\xi}{2}\frac{\partial f}{\partial \xi} = \alpha_L \frac{\partial^2 f}{\partial \xi^2} \tag{3.5}$$

Using separation of variables, we use the general solution for f' [8],

$$\frac{\partial f}{\partial \xi} = A_0 e^{-\frac{\xi^2}{4\alpha_L}} \tag{3.6}$$

for some constant A_0. Integrating this solution yields a similarity solution of the heat equation

$$u_L(x,t) = f(\xi) = f(x/\sqrt{t}) = A_1 + A_0 \int_0^{x/\sqrt{t}} e^{-\frac{s^2}{4\alpha_L}} ds \tag{3.7}$$

$$= A_1 + A_2 \int_0^{x/\sqrt{4\alpha_L t}} e^{-z^2} dz, \tag{3.8}$$

for some constants A_1, A_2. For convenience, we have substituted $s = \sqrt{4\alpha_L} z$. Additionally, we recognize the error function, which is defined as

$$\text{erf}(z) = 1 - \text{erfc}(z) = \frac{2}{\sqrt{\pi}} \int_0^z e^{-t^2} dt \quad \text{and} \quad \frac{d}{dz}\text{erf}(z) = \frac{2}{\sqrt{\pi}} e^{-z^2} \tag{3.9}$$

Using this definition, we can express $u_L(x,t)$ as

$$u_L(x,t) = A + B\,\text{erf}\left(\frac{x}{2\sqrt{\alpha_L t}}\right), \tag{3.10}$$

for some constants A and B. Now, using the boundary condition for $u_L(x,t)$ at $x = 0$, we obtain

$$A = T_L$$

Applying the boundary condition at the phase interface subsequently yields

$$T_m = T_L + B\,\text{erf}\,(\lambda) \tag{3.11}$$

where we define the parameter λ as

$$\lambda = \frac{s(t)}{2\sqrt{\alpha_L t}} \tag{3.12}$$

As condition (3.11) has to be true for all values of t, λ needs to be constant. Solving Equation (3.11) for B, we obtain

$$B = \frac{T_m - T_L}{\text{erf}\,(\lambda)}$$

Substituting the values found for A, B and λ into Equation (3.10) yields a general solution for $u_L(x,t)$, as seen in Equation (3.13). In similar fashion, the solution for $u_S(x,t)$ may be obtained, as is depicted in Equation (3.14) [10].

$$u_L(x,t) = T_L + (T_m - T_L)\frac{\text{erf}\left(\frac{x}{2\sqrt{\alpha_L t}}\right)}{\text{erf}(\lambda)} \tag{3.13}$$

$$u_S(x,t) = T_S + (T_m - T_S)\frac{\text{erfc}\left(\frac{x}{2\sqrt{\alpha_S t}}\right)}{\text{erfc}\left(\lambda\sqrt{\frac{\alpha_L}{\alpha_S}}\right)} \tag{3.14}$$

If we substitute Equation (3.12) in the left hand side of Equation (3.1c), we find

$$L\rho\frac{\partial s}{\partial t} = 2\lambda L\rho\frac{\partial}{\partial t}\sqrt{\alpha_L t} = \lambda L\rho\frac{\sqrt{\alpha_L}}{\sqrt{t}} \tag{3.15}$$

For convenience, we split the right hand side of Equation (3.1c) into parts of $u_L(x,t)$ and $u_S(x,t)$. Substituting Equation (3.13) into the corresponding equation for $u_L(x,t)$ and the derivative of the error function as shown in Equation (3.9) gives

$$\begin{aligned} k_L\left.\frac{\partial u_L}{\partial x}(x,t)\right|_{x=s(t)} &= k_L\frac{\partial}{\partial x}\left(\frac{(T_m-T_L)}{\operatorname{erf}(\lambda)}\operatorname{erf}\left(\frac{x}{2\sqrt{\alpha_L t}}\right)+T_L\right)\Bigg|_{x=s(t)} \\ &= k_L\frac{(T_m-T_L)}{\operatorname{erf}(\lambda)}\frac{2}{\sqrt{\pi}}e^{-\frac{s(t)^2}{4\alpha_L t}} \\ &= k_L\frac{(T_m-T_L)}{\operatorname{erf}(\lambda)}\frac{2}{\sqrt{\pi}}e^{-\lambda^2} \end{aligned} \tag{3.16}$$

Similarly, for Equation (3.14), we obtain

$$k_S\left.\frac{\partial u_S}{\partial x}(x,t)\right|_{x=s(t)} = -k_S\left(\frac{\alpha_L}{\alpha_S}\right)^{\frac{1}{2}}\frac{(T_m-T_S)}{\operatorname{erfc}\left(\lambda\left(\frac{\alpha_L}{\alpha_S}\right)^{\frac{1}{2}}\right)}\frac{2}{\sqrt{\pi}}e^{-\lambda^2\left(\frac{\alpha_L}{\alpha_S}\right)} \tag{3.17}$$

Substituting Equations (3.15 - 3.17) into Equation (3.1c) yields [10, 11]

$$\frac{e^{-\lambda^2}}{\operatorname{erf}(\lambda)}+\frac{k_S}{k_L}\left(\frac{\alpha_L}{\alpha_S}\right)^{\frac{1}{2}}\frac{T_m-T_S}{T_m-T_L}\frac{e^{-\lambda^2(\alpha_L/\alpha_S)}}{\operatorname{erfc}\left(\lambda(\alpha_L/\alpha_S)^{1/2}\right)} = \frac{\lambda L\sqrt{\pi}}{c_p(T_m-T_L)} = \lambda\beta\sqrt{\pi}, \tag{3.18}$$

from where we see the importance of the Stefan number. The value for λ may be numerically approximated using the Newton-Raphson method, which is discussed in Section 5.1. Henceforth, using thermal properties of the substance that undergoes a phase transition, a value for λ may be found, with which the location of the one-dimensional moving boundary can be determined using the equation

$$s(t) = 2\lambda\sqrt{\alpha_L t} \tag{3.19}$$

which is deducted from Equation (3.12). This solution is often called the Neumann solution after Franz Neumann, who first solved this problem in 1860 [12]. This equation shows that the location of the moving boundary is proportional to the square root of time. In Figure 2, this behaviour can be seen for different values of λ. For this showcase, an arbitrary constant value of $\alpha_L = 1$ is taken.

For multi-dimensional Stefan problems, the analytic solution can generally not be found due to its complexity. Therefore, we will focus on investigating numerical methods that can solve multidimensional Stefan problems. We will discuss a numerical method for one-dimensional systems, which we will extend for multi-dimensional systems. In these cases, we assume the location of the interface to be where the temperature is equal to T_m, the melting temperature of the substance.

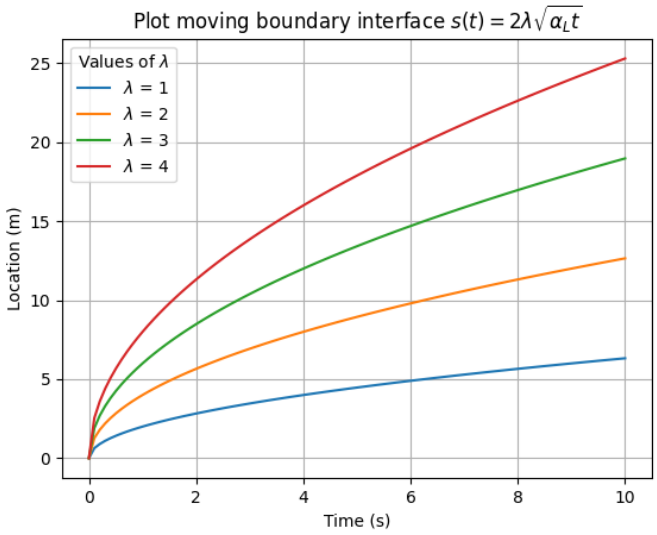

FIGURE 2: The behaviour of Equation (3.19) for different values of λ

4 Enthalpy method for the Stefan problem

In the preceding section, an analytical solution was found for the one-dimensional two-phase Stefan problem. It is also mentioned that for multi-dimensional systems, an analytical solution is not feasible. For this reason, we are obliged to look into numerical methods that can closely represent the exact result. To make sure that applying the numerical methods is not complex, we rewrite the Stefan problem into a more convenient formulation. There are various of such methods used for reformulating the moving boundary problem [13, 14, 15].

In this chapter, we will look into the so-called enthalpy method. The enthalpy method introduces an enthalpy function that represents the total internal energy of the system. By tracking the enthalpy, the method captures the phase transition and energy redistribution that occurs in the system. In the enthalpy function, there is a jump discontinuity across the moving boundary, representing the change in enthalpy that is associated with the phase transition. We will refer to enthalpy as H, the enthalpy per unit mass. Alternatively, it is often referred to enthalpy as the total enthalpy per unit volume, denoted as E. The main difference between these two notations is the presence of the density ρ, corresponding to the role of ρ in the relation between mass and volume. In this study, we prefer the H-notation.

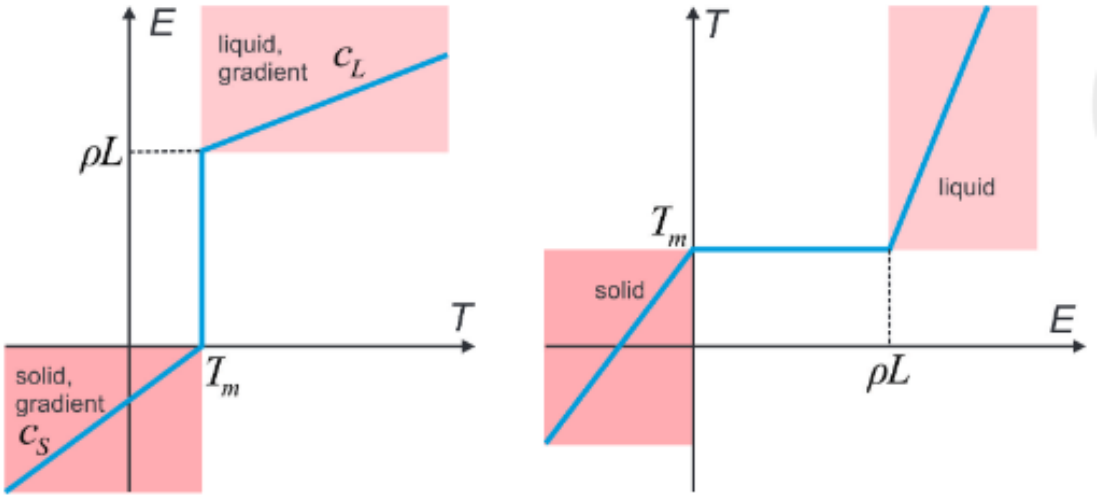

FIGURE 3: Relation between enthalpy per unit volume E with respect to temperature T and its inverse temperature T as a function of E [16]. Note that in this specific figure, E denotes the enthalpy, hence the presence of ρ alongside the latent heat L

4.1 Mathematical formulation

It has been shown [10, 17] that the heat conduction equation can rewritten in an enthalpy form as such:

$$\rho\frac{\partial H(T)}{\partial t} - \frac{\partial \phi}{\partial x} = 0 \quad \text{or} \quad \nabla \cdot (k\nabla T) = \rho\frac{\partial H(T)}{\partial t} \tag{4.1}$$

where again, Fourier's law has been utilized. Note that here, $T(x,t)$ is used instead of $u(x,t)$, to underline that this is a function of the heat distribution. Moreover, the enthalpy

$H(x,t)$ is said to be [10, 18]

$$H(x,t) = \begin{cases} \int_{T_m}^{T(x,t)} c_p(\tau)d\tau + L & \text{for} \quad T(x,t) > T_m \\ \int_{T_m}^{T(x,t)} c_p(\tau)d\tau & \text{for} \quad T(x,t) < T_m \end{cases} \tag{4.2}$$

which is referred to as the enthalpy formulation. We can now see the role of the latent heat. Once the substance has changed phase, the total internal energy changes with a value L, which is exactly the definition of latent heat. For constant c_p, this is equivalent to

$$H(T) = \begin{cases} c_p(T - T_m) & \text{for} \quad T < T_m \\ c_p(T - T_m) + L & \text{for} \quad T > T_m \end{cases} \tag{4.3}$$

Conversely, in terms of the enthalpy as a function of temperature,

$$T = \begin{cases} T_m + \dfrac{H}{c_p} & \text{for} \quad H < 0 \\ T_m & \text{for} \quad 0 \leq H \leq L \\ T_m + \dfrac{H - L}{c_p} & \text{for} \quad H > L \end{cases} \tag{4.4}$$

In Figure 3, the relation between enthalpy and temperature for isothermal phase changes may be found. It can be seen that, at melting temperature T_m, the enthalpy jumps with the value L, the latent heat, as is expected from Equation (4.4). It should be noted that formally, the specific heat of a liquid and solid are different. For simplicity reasons, we assume that this value stays constant throughout the phase transition.

5 Numerical methods

In this chapter, we present the main numerical algorithms that are used in this study. In Section 5.1, we first discuss the iterative method that is used to obtain a solution for the transcendental equation for λ, as seen in Equation (3.18). In Section 5.2, we provide the reader with an overview of the main steps that are taken in the simulation process, to make sure that the structure of our methodology is clear to the reader. In Section 5.3, we discuss the finite difference method, that is used to discretize the enthalpy formulation which was introduced in the previous chapter. We continue in Section 5.3.1 by presenting an integration method that is used to solve the discretized system. Throughout Section 5.3, we discuss the accuracy of our chosen numerical methods. We conclude this chapter with a remark regarding multi-dimensional systems.

5.1 Newton-Raphson method

In Section 3.1, a transcendental equation for λ was introduced. The values of this λ can be calculated by utilizing the Newton-Raphson method. This method is a root-finding algorithm which provides accurate approximations to the roots of real-valued functions. Starting with an estimate for the root x_0, Equation (5.1) is used to determine more accurate approximations:

$$x_{n+1} = x_n - \frac{f(x_n)}{f'(x_n)} \quad \text{for } n = \{0, 1, \dots\} \tag{5.1}$$

The preceding equation will be iterated until

$$|x_{n+1} - x_n| < \epsilon \quad \text{for some sufficiently small } \epsilon > 0$$

As will be discussed in Section 6.1, the parameters that are used in the transcendental equation in the case of paraffin are denoted in Table 1. For mathematical convenience, it is assumed that $k_L = k_S$ and $\rho_L = \rho_S$. In Equation (3.18) only a ratio is necessary for these values, thus we will not include them in this section, with an exception for $c_L = c_S = c_p$, as this value is necessary for the Stefan number.

TABLE 1: Parameters used in Equation (3.18) for the calculation of λ in paraffin

Symbol	Value	Unit
c_p	2.14	kJ kg^{-1}K^{-1}
L	168	kJ kg^{-1}
T_L	85	°C
T_m	45	°C
T_S	20	°C

5.2 Sequential steps in simulation process

In this section, we provide the reader with an overview about the sequential steps that are taken in the simulation process. The workflow has the same order as this study, as is illustrated in Figure 4. We first define the problem that we want to tackle, after which we formulate it mathematically, as has been done in Chapters 2 and 4. In Chapter 5, we discretize the Stefan problem and solve it using an appropriate time integration method.

The workflow ends at the simulation, where the obtained results will be discussed and validated.

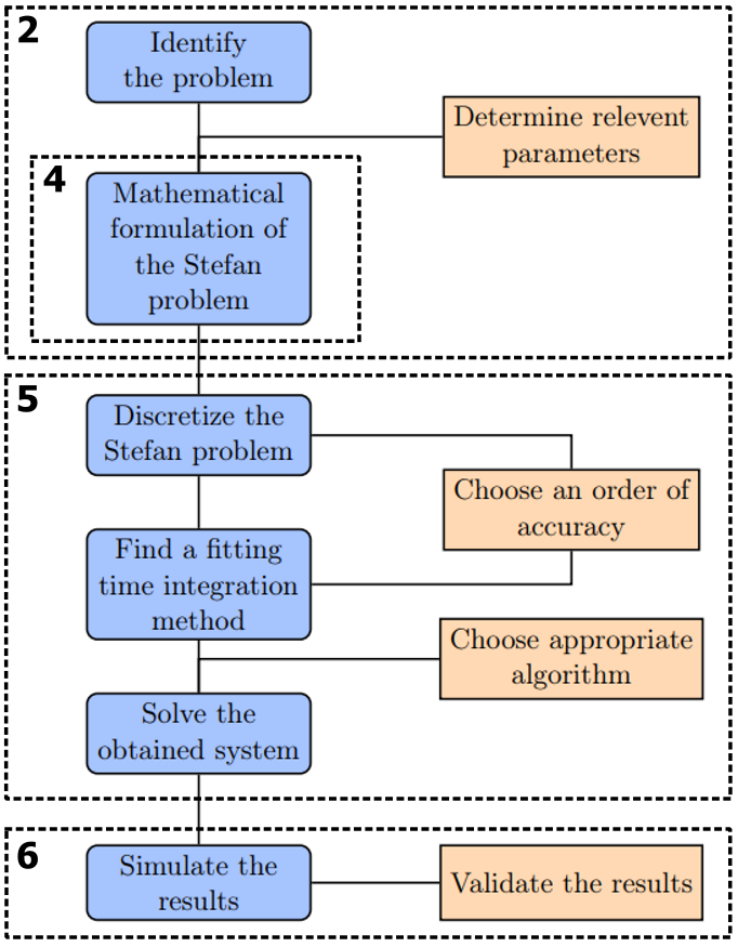

FIGURE 4: The workflow of simulating the Stefan problem

5.3 Finite difference method

The finite difference method is a numerical technique to approximate solutions of differential equations. This is done by dividing the domain of interest into a series of space and time grid points, denoted by (x_i, t^n) for the one-dimensional case. The finite difference method tackles differential equations by replacing their derivatives with finite difference approximations. These substitutions subsequently yield a set of algebraic equations, which can be solved using appropriate algorithms. In this section, we will discuss general difference equations for discretizing continuous systems and explore key concepts, including the truncation error and the order of accuracy associated with these difference equations.

We obtain the difference equations utilizing Taylor's theorem with remainder. The Taylor series expansion yields

$$f(x+h) = f(x) + hf'(x) + h^2 \frac{f''(\zeta)}{2!} \quad \text{for } \zeta \in [x, x+h]$$

After rearranging, we recognise the definition of the derivative of $f(x)$. Now, from Equation (5.2), we can see that the error is correlated to h.

$$\frac{f(x+h)-f(x)}{h} - f'(x) = h\frac{f''\zeta)}{2!} \quad \text{for } \zeta \in [x, x+h] \tag{5.2}$$

If we let $h = \Delta x > 0$ for finite Δx and denote the error with the Big-O notation, we obtain

$$\left.\frac{\partial f}{\partial x}\right|_{x_i} = \frac{f(x_i+\Delta x)-f(x_i)}{\Delta x} + O(\Delta x) \tag{5.3}$$

which is called the forward difference equation, with a first-order error $O(\Delta x)$. Similarly, if we let $h = -\Delta x < 0$ for finite Δx, we obtain

$$\left.\frac{\partial f}{\partial x}\right|_{x_i} = \frac{f(x_i)-f(x_i-\Delta x)}{\Delta x} + O(\Delta x) \tag{5.4}$$

which is the backward difference equation, also with first-order truncation error $O(\Delta x)$. We now sum the Taylor expansions of $f(x+\Delta x)$ and $f(x-\Delta x)$, which results in the central difference equation

$$\left.\frac{\partial f}{\partial x}\right|_{x_i} = \frac{f(x_i+\Delta x)-f(x_i-\Delta x)}{2\Delta x} + O(\Delta x^2) \tag{5.5}$$

Note that this difference equation has a second-order error, $O(\Delta x^2)$, which would make this equation the most accurate of the three. In a similar fashion as presented above, the difference equation for higher-order differential equations can be constructed.
To compute accurate results that closely represent the exact solution, we have two main options. As implied by Equation (5.2), the numerical approximation converges to the exact solution as $h \to 0$. Hence, the first option is to take sufficiently small spatial and temporal steps so that even with high truncation errors, we converge to the exact solution. Unfortunately, this is computationally only possible up to a certain point, as the simulation would take a very long time for infinitesimal step sizes.

The second option is to decrease the truncation error. This can be done by using more accurate difference equations by taking more adjacent grid points into account. To be able to see whether the accuracy may be improved, we have to know the accuracy of the used numerical approximation. We formally refer to the truncation error as $O\left(h^{p+1}\right)$, where p is called the order of convergence. Hence, to obtain the truncation error, we have to find the order of convergence. We consider the convergence quotient Q. For sufficiently small h, we have

$$Q = \frac{y(4h)-y(2h)}{y(2h)-y(h)} = 2^p \tag{5.6}$$

Hence, we can find the order of convergence by $p = 2\log(Q)$.

5.3.1 Forward Euler method

In this section, we will discuss the Forward Euler scheme. This is a time integration method for solving differential equations. On the domain $\Omega = \{(x,t) \in \mathbb{R}^2 \,|\, 0 < x \leq N,\, t > 0\}$, we let Δx and Δt denote the spatial grid size and temporal step, respectively. We consider

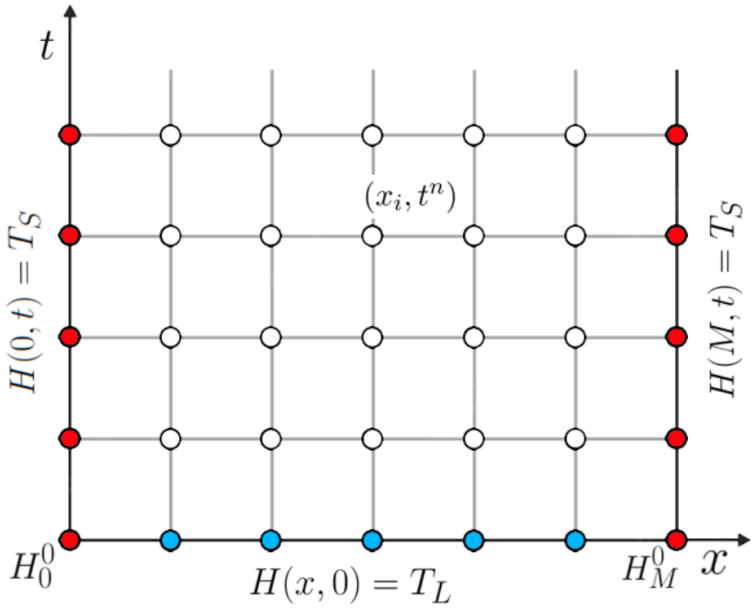

FIGURE 5: Graphical overview of the grid points (x_i, t^n) in a Forward Euler scheme, including initial values and boundary conditions.

the spatial domain to be uniformly parted into M cells. Ultimately, we obtain the grid points (x_i, t^n) which are defined as

$$x \to x_{i+1} = x_i + i\Delta x \quad \text{for } i = 0, 1, \ldots, M$$
$$t \to t^{n+1} = t^n + n\Delta t \quad \text{for } n = 0, 1, \ldots$$

In Figure 5, a domain is illustrated that includes grid points (x_i, t^n). As said in the preceding sections, we will be using the enthalpy method to obtain numerical solutions. Recall from Section 4 that the mathematical formulation of the enthalpy method is

$$\frac{\partial H}{\partial t} = \alpha \frac{\partial^2 T}{\partial x^2} \tag{5.7}$$

We approximate Equation (5.7) by using the forward difference approximation for the time derivative and the center difference approximation for the space derivative. Additionally, we denote the numerical approximations of H and T at grid points (x_i, t^n) as H_i^n and T_i^n, respectively. This yields the numerical equation

$$\frac{H_i^{n+1} - H_i^n}{\Delta t} = \alpha \frac{T_{i+1}^n - 2T_i^n + T_{i-1}^n}{(\Delta x)^2} \tag{5.8}$$

Solving the equation for H_i^{n+1} yields

$$H_i^{n+1} = H_i^n + \gamma \left(T_{i+1}^n - 2T_i^n + T_{i-1}^n \right), \quad \text{where} \quad \gamma = \alpha \frac{\Delta t}{(\Delta x)^2} \tag{5.9}$$

Realizing H_i^n is dependent on the value T_i^n, we introduce $F(H_i^n) = T_i^n$. Hence, we may rewrite the aforementioned equation to

$$H_i^{n+1} = H_i^n + \gamma \left(F(H_{i+1}^n) - 2F(H_i^n) + F(H_{i-1}^n) \right), \quad \text{where} \quad \gamma = \alpha \frac{\Delta t}{(\Delta x)^2} \tag{5.10}$$

Hence, a solution for H_i^{n+1} may be computed if $H_{i+1}^n, H_i^n, H_{i-1}^n$ are known. This dependency is illustrated in the stencil in Figure 6. In this figure, weights are given with the color red. The weights in a stencil are assigned to adjacent grid points, that determine the influence of each adjacent grid point in calculating the value of the new grid point. By Figure 5, it may be seen that using the mentioned stencil, all values for H_i^n may be computed, provided some initial and boundary conditions are introduced. In the case of our model, we let the initial value be the temperature at x_0, which is T_L. For the boundary conditions, we set $H_1^n = H_M^n = T_S$, the initial temperature of the solid substance.

In matrix form, Equation (5.10) is equivalent to

$$H^{n+1} = I_M H^n - AF(H^n) \tag{5.11}$$

where H^n represents a vector of length M that corresponds to values of H_i^n. Recall that the function $F : \mathbb{R}^{M\times 1} \to \mathbb{R}^{M\times 1}$ is defined as $F(H_i^n) = T_i^n$. Following Equation (5.10), I_M denotes the $M \times M$ identity matrix, and A denotes a tridiagonal matrix given by

$$A = \begin{bmatrix} 2\gamma & -\gamma & 0 & \dots & 0 \\ -\gamma & 2\gamma & -\gamma & \ddots & \vdots \\ 0 & \ddots & \ddots & \ddots & 0 \\ \vdots & \ddots & -\gamma & 2\gamma & -\gamma \\ 0 & \dots & 0 & -\gamma & 2\gamma \end{bmatrix} \tag{5.12}$$

Letting $I_M H^n - AF(H^n) = BH^n$ for some matrix B, we can see that

$$H^{n+1} = BH^n \tag{5.13}$$

which can be iteratively solved for all grid points (x_i, t^n).

By the Von Neumann stability analysis, we know that the Forward Euler method is conditionally stable, i.e. for the Forward Euler method to be stable, we must have sufficiently small time steps Δt such that

$$\gamma = \alpha \frac{\Delta t}{(\Delta x)^2} \leq \frac{1}{2} \quad \text{or} \quad \Delta t \leq \frac{(\Delta x)^2}{2\alpha} \tag{5.14}$$

Henceforth, to retain the stability of the Forward Euler method, we determine the time step Δt such that it depends on spatial step size Δx and thermal diffusivity α and yields a stable time integration of the discrete problem.

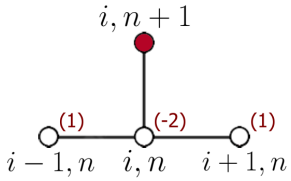

FIGURE 6: Stencil of the Forward Euler method. The weights are denoted in red.

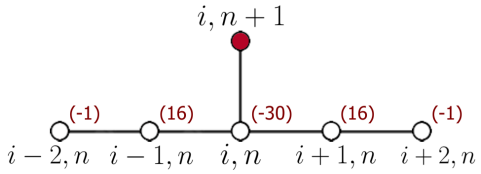

FIGURE 7: Five-point stencil for one-dimensional application. The weights are denoted in red.

5.3.2 Accuracy of Forward Euler method

As mentioned, numerical methods converge to the exact solution when $\Delta x \to 0$, yet still have truncation errors. In Section 5.3, we investigated the truncation error for the general difference equations. For the Forward Euler method as illustrated in Equation (5.8), the truncation error is of second-order. It was mentioned that there are two main methods to increase the accuracy of the Forward Euler method. The least complex method is decreasing the spatial and time steps. The alternative is by adopting a different stencil than the one that was illustrated in Figure 6. A concrete alternative is presented in Figure 7. In this figure, a five-point stencil is presented. In comparison with the three-point stencil as in Figure 6, this stencil takes two additional adjacent grid points into account. If more adjacent grid points are taken into account to calculate new values, the stencil becomes a more accurate method. For this study, we consider the stencil as presented in Figure 6 to be reasonably accurate, as we take sufficiently small spatial and temporal steps.

5.4 Multi-dimensional numerical analysis

The goal of this study is to obtain a model that predicts the evolving temperature distribution as a function of space and time in a phase-change material. Even though it is possible to draw valid conclusions from one-dimensional simulations, multi-dimensional simulations offer a significant increase in the ability to draw more relevant conclusions for the application at hand. For this reason, we also introduce the numerical systems that are necessary to approximate two- and three-dimensional solutions.

5.4.1 N-Dimensional systems

For convenience, we only show the two-dimensional discretization. For the three-dimensional system, a similar approach may be used. The enthalpy formulation that correspond to a two-dimensional system is

$$\frac{\partial H}{\partial t} = \alpha \left(\frac{\partial^2 T}{\partial x^2} + \frac{\partial^2 T}{\partial y^2} \right) \tag{5.15}$$

Substituting the difference equations as in the one-dimensional case, we obtain

$$\frac{H_{i,j}^{n+1} - H_{i,j}^{n}}{\Delta t} = \alpha \left(\frac{T_{i+1,j}^{n} - 2T_{i,j}^{n} + T_{i-1,j}^{n}}{(\Delta x)^2} + \frac{T_{i,j+1}^{n} - 2T_{i,j}^{n} + T_{i,j-1}^{n}}{(\Delta y)^2} \right) \tag{5.16}$$

For mathematical convenience we let the spatial step size in the x and y direction be of equal length, i.e., $\Delta x = \Delta y = \Delta\delta$. Using again $F(H_{i,j}^{n}) = T_{i,j}^{n}$, we obtain the numerical approximation

$$H_{i,j}^{n+1} = H_{i,j}^{n} + \bar{\gamma} \left(F\left(H_{i+1,j}^{n}\right) + F\left(H_{i-1,j}^{n}\right) + F\left(H_{i,j+1}^{n}\right) + F\left(H_{i,j-1}^{n}\right) - 4F\left(H_{i,j}^{n}\right) \right) \tag{5.17}$$

$$\text{with} \quad \bar{\gamma} = \alpha \frac{\Delta t}{\Delta \delta^2} \tag{5.18}$$

The stencil that is used for this two-dimensional system is illustrated in Figure 8. Similar to the one-dimensional case, the two-dimensional case may be iteratively solved by using the initial values and boundary conditions. Similar to the one-dimensional case, more enhanced stencils may improve the accuracy of the two-dimensional approximation.

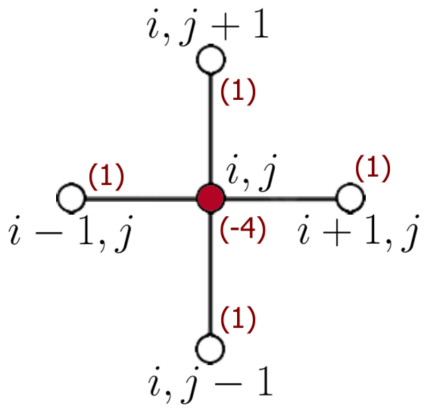

FIGURE 8: Stencil of the two-dimensional Forward Euler method. The weights are denoted in red.

6 Simulation and validation

In the preceding chapters, we have presented the physical and mathematical foundations underlying phase change problems. We used this to discuss both analytical and numerical methods to obtain solutions for the two-phase Stefan problem. Specifically, we were able to derive an exact solution for the one-dimensional case using an analytical approach. We will utilize the exact solution to investigate the accuracy of the chosen numerical methods for the one-dimensional case, from which we may draw some conclusions regarding the accuracy of the multi-dimensional cases.

Recall that this study is based on the distribution of heat in phase change materials. Consequently, before we are able to simulate anything, we provide the reader with some essential parameters that are used to replicate these materials. This is done in Section 6.1. Subsequently, we will talk about the one-dimensional implication of the Stefan problem. We start by validating the numerical approximation using the exact solution and convergence analysis. We end this section by performing sensitivity analysis on the parameters, to determine the influence of a change in parameters on the system.
In Section 6.3, we look into the two-dimensional simulations for systems with adiabatic and non-adiabatic boundary conditions. This is done to provide the reader with a validation of the two-dimensional implication. We end this chapter with the application of nanofillers to phase change materials. In this chapter, we investigate the effect of graphene nanofillers on the performance of phase change materials. Recall that the application of graphene nanofillers will be realised as a mixture between graphene and paraffin, which will be assumed to be a homogeneous substance.

6.1 Simulation parameters

As seen in the models presented in Sections 3 and 5, parameters are necessary in order for the simulations to represent the desired physical system. It is mentioned that these parameters depend on the thermal properties of the substance. These properties are:

Density ρ

Thermal conductivity k

Specific heat capacity c_p

Latent heat L

These values are used to calculate the thermal diffusivity, α, which is defined by

$$\alpha = \frac{k}{\rho c_p} \tag{6.1}$$

In this study, we are interested in the case of organic phase change materials. Specifically, we are interested in paraffin as the phase change material. As different kinds of paraffin yield different thermal properties, we use values based on previous research [3, 19, 20], as seen in Table 2. Although the chosen parameters are indications rather than exact representations, they are expected to closely resemble the behaviour of paraffin with minor deviations. It is important to note that the focus of our study lies in understanding the heat distribution within phase change materials. While further refinement may be necessary for a more precise replication of the behaviour of paraffin, the parameters used in this study provide a solid starting point for our simulations and analysis.

TABLE 2: Parameters used for the simulation of the thermal behaviour of paraffin

Symbol	Value	Unit
ρ	900	kg m^{-3}
k	0.2	W $m^{-1}K^{-1}$
c_p	2.14	kJ $kg^{-1}K^{-1}$
L	168	kJ kg^{-1}

To compensate the low thermal conductivity of paraffin, nanofillers with a much higher conductivity could be added to improve the overall properties of the heat transfer throughout the phase change material. For this study, we consider graphene. We assume the mixture between graphene and paraffin to be a homogeneous substance. It has been shown that the addition of graphene yields significant improvements at the thermal conductivity, while reducing latent heat and density [5, 6, 21]. The parameters that will be used for simulations regarding the mixture of paraffin and graphene nanofillers are displayed in Table 3. Note that these parameters are also indications, determined for simulation and analysis purposes. We will only consider the addition of nanofillers for two-dimensional simulation.

TABLE 3: Parameters used for the simulation of the thermal behaviour of graphene

Symbol	Value	Unit
ρ	900	kg m^{-3}
k	1	W $m^{-1}K^{-1}$
c_p	2	kJ $kg^{-1}K^{-1}$
L	150	kJ kg^{-1}

Additionally, we are interested in the phase transition from solid to liquid. To be able to model this, initial temperatures and a melting temperature is necessary for simulation. For mathematical convenience, to showcase the behaviour of the phase change material, the following temperatures are chosen.

$$T_L = 80°C$$
$$T_m = 45°C$$
$$T_S = 20°C$$

Recall that here, T_L denotes the temperature that is produced by the heat source. For example, if phase change material is mounted in walls to absorb heat, the heat produced by the sun and its radiation may be seen as the heat source. T_m denotes the melting temperature of the material. T_S denotes the temperature of the solid, which occurs when the substance reaches a state of complete cooling equilibrium.

6.2 One-dimensional implication

In respectively Sections 3 and 5, an analytical and a numerical solution of the moving boundary condition was discussed. We now look into the different results that were obtained by the simulations. We will validate the found results and perform parameter sensitivity analysis on the simulations to get a better insight in the accuracy and validation of the numerical approximation.

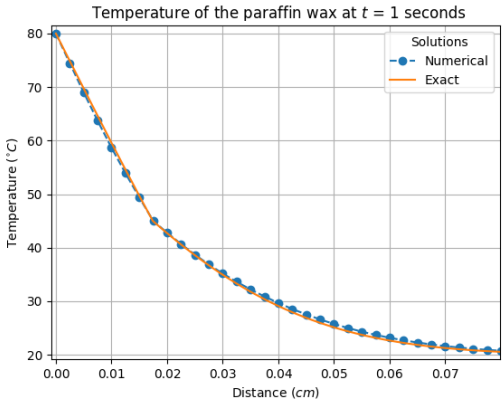

FIGURE 9: Comparison numerical approximation to analytical solution: Behaviour of heat distribution over distance

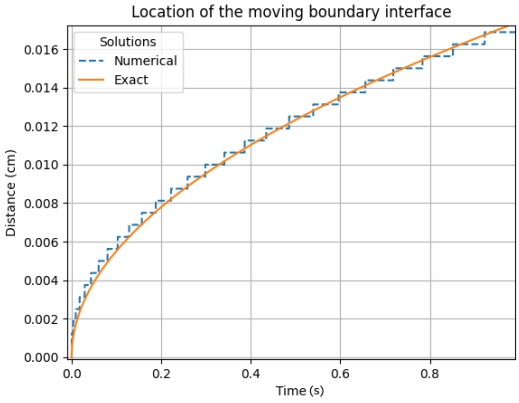

FIGURE 10: Comparison numerical approximation to analytical solution: Tracking the phase-change boundary over time

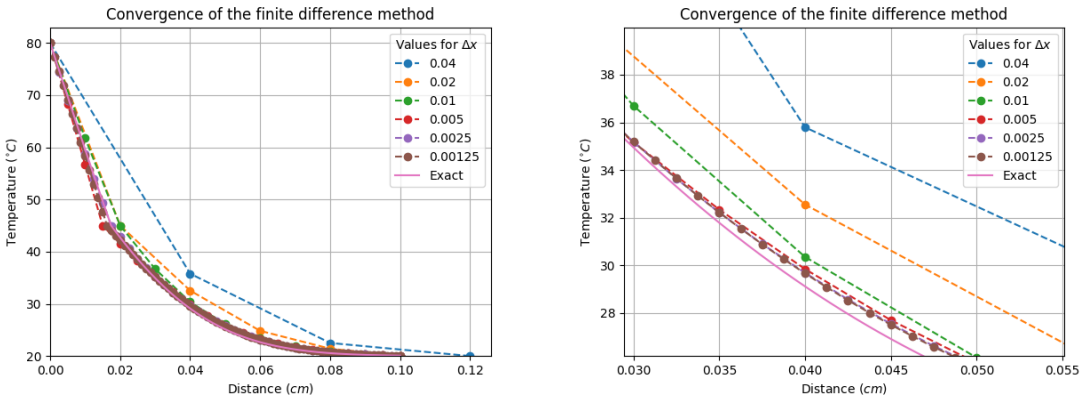

FIGURE 11: The convergence of a numerical approximation for decreasing space-time steps

6.2.1 Validation of general one-dimensional system

In this section, the general behaviour of the finite difference method is determined. In Figure 9, the temperature over the distance of the object is shown for various time frames. Additionally, the location of the moving boundary is illustrated. The behaviour of the analytical and numerical solution is, as expected, similar. The observed correlation between the two solutions suggests that the numerical method effectively approximates the exact solution for the given problem. These findings give the first confidence that the numerical method is correctly chosen and implemented.

6.2.2 Convergence analysis of numerical methods

As mentioned in Section 5, numerical methods should converge to the corresponding analytical solution, when the space-time size steps converge to zero. To see whether this is true in the case of the one-dimensional simulation, multiple simulations are provided in Figure 11, that show the numerical approximation for increasingly smaller space-time size

TABLE 4: Numerical values and its errors

Δx	Value	Q
0.04	35.789	-
0.02	32.456	-
0.01	30.347	1.474
5e-3	29.836	4.303
2.5e-3	29.678	3.234
1.25e-3	29.653	6.320

steps. Indeed, a convergence to the analytical solution can be seen. Recall that the time size Δt behaves accordingly with Δx via Equation (5.14). Hence, if Δx decreases, Δt decreases.

Additionally, in the right figure of Figure 11, a zoomed illustration is shown. Here, it may be more clear that the numerical solution increasingly gives more accurate approximates of the analytical solution. In Table 4, the values of the numerical approximation at distance $x = 0.040$ are denoted. If we determine the convergence quotient Q as in Equation (5.6), we see that Q does not seem to converge to a clear value, while a value of $Q = 2$ was expected. Nevertheless, we do see that the values are slowly converging to a certain value. Hence, even though there is not concrete proof that validates the theoretical truncation error of 2 as discussed in Section 5.3.2, the numerical method still seems to converge to the exact solution.

6.2.3 Parameter sensitivity analysis and performance evaluation

Here, we will turn our attention to the influence of a change in thermal properties of the phase change material. The simulations illustrated in Figures 9 and 10 show the behaviour of the system with the parameters as denoted in Table 2. In the case that a different type of substance will be used as phase change material, the behaviour of the material might differ. This change in behaviour might yield improvements or deterioration of how fast energy may be stored in the substance.

We will first determine the influence of the melting temperature T_m. Next, we investigate the influence of the thermal diffusivity α, by changing each individual component k, c_p and ρ. Finally, we will look at the effect of the latent heat L. For this section, we will only look at the exact solution, opposing to the numerical solution. This is because we are interested in how a change of parameters changes the behaviour of the system, rather than emphasizing the accuracy of the numerical method.

In Figure 12, simulations for different melting temperatures T_m may be observed. It can be seen that for each melting temperature, the moving boundary interface appears on the same location. This implies that a change in melting temperature does not have any influence on the speed of transitioning the substance. In Figure 13, the effect of a different conductivity can be seen. We see a clear change in the speed with which the substance transitions to a different state of matter. A similar result may be seen in Figures 14 and 15, which is expected due to the equation of the thermal diffusivity, as seen in Equation (6.1). Lastly, we look at the change in the latent heat. A lower latent heat means that less energy is required to transition to change phase. Therefore, it is expected that for a lower latent heat, the phase change process would occur more rapidly throughout the material.

This is exactly what can be observed from Figure 16.

To improve the time which with the phase transitions occur as quickly as possible (i.e. solid to liquid transition), we see that we can change a lot of thermal properties. The one thermal property which is not of interest is the melting temperature, as this seems to have no influence on the phase transition process. In previous studies, it is shown that the effect of graphene nanofillers has more influence on the thermal conductivity of phase change materials compared to other thermal properties [5, 6, 21]. Comparing the found improvements that are shown in said studies with our simulations, we can confidently say that these adjustments should indeed increase the speed with which the phase transitions occur.

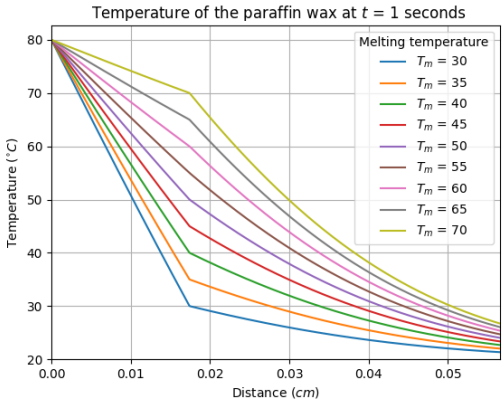

FIGURE 12: Effect of different values of melting temperature T_m

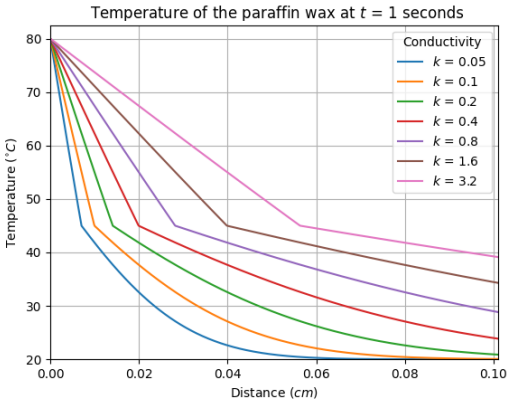

FIGURE 13: Effect of different values of conductivity k

6.3 Two-dimensional implication

In this section, we will investigate the heat distribution in two-dimensional systems, where we look into the behaviour of adiabatic and non-adiabatic systems. With adiabatic systems, we refer to a system with adiabatic boundary conditions. In adiabatic boundary conditions, the heat flux at the boundary is set to zero. This replicates a insulated boundary. In non-adiabatic systems, this is not the case. In these systems, heat might escape through the boundary, which results in a nonzero heat flux.

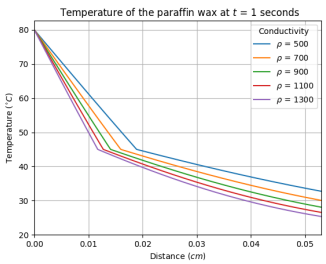

FIGURE 14: Effect of different values of density

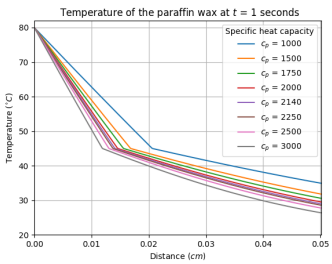

FIGURE 15: Effect of different values of specific heat capacity

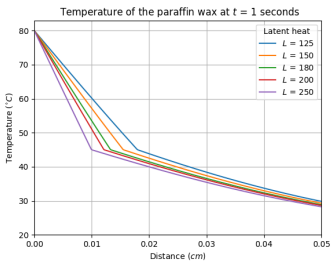

FIGURE 16: Effect of different values of latent heat

6.3.1 Heat distribution in adiabatic system

We first look at an adiabatic system. As no energy should escape from the boundaries, we expect every one-dimensional slice, that starts from the heat source of system, to be equal. In Figure 17, three different frames from the heat distribution are taken. Throughout these frames, the development of the heat can be clearly seen. As expected, the heat spreads uniformly throughout the substance. This implies that the adiabatic boundary conditions are implemented correctly.

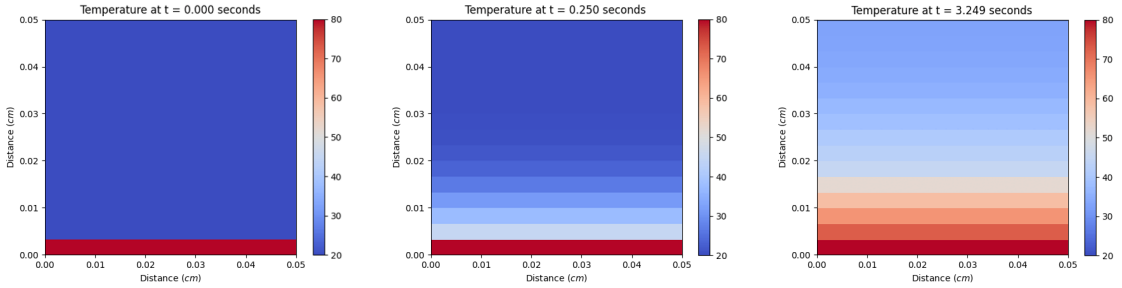

FIGURE 17: Uniform distribution throughout an adiabetic system

To determine the validity of this simulation, we take a slice at an arbitrary place and compare this with the one-dimensional system as presented in preceding section. For validation, we take a slice at $t = 1$ seconds at an arbitrary location. This slice is illustrated in Figure 19, together with the exact solution. If we compare this slice with the one-dimensional simulation in Figure 9, we can see a very similar heat distribution. This validates that the two-dimensional system was implemented correctly.

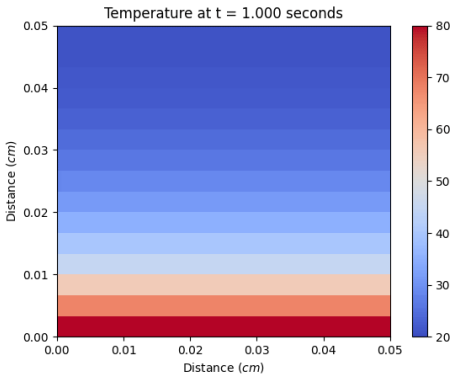

FIGURE 18: A uniform heat distribution through the substance at $t = 1$ seconds.

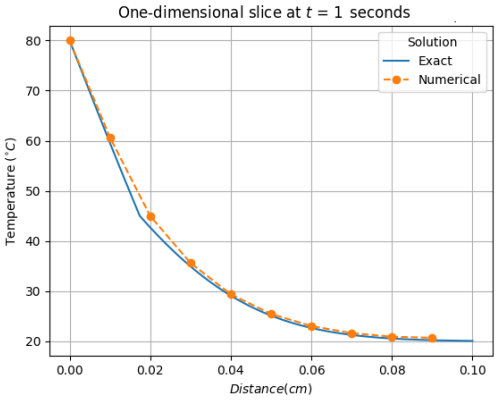

FIGURE 19: Comparison of a slice of the two-dimensional implication and the exact solution

6.3.2 Heat distribution and geometric properties of non-adiabatic systems

In this section, we will investigate non-adiabatic systems and look closely at its geometric properties. The distribution of heat should behave the same when exposed to the same conditions. We first look at the symmetry of heat distribution. In Figures 20 - 23, a heat

source is applied at different locations. Lines are added in the first two figures as an overlay to act as a reflection axis.

First, a heat source is added to the bottom, similar to preceding section. In Figure 20, we can see that the heat does not spread uniformly, but rather loses heat at the sides. This is a clear indication that the boundaries are indeed non-adiabatic, as there is a nonzero heat flux. Secondly, a heat source is added in the corner. In Figure 21, we can see how the heat spreads diagonally and is symmetric along the diagonal reflection axis. A similar behaviour can be observed in Figure 22, where a source is added at all sides. To conclude, we have Figure 23, where a heat source was added in the centre of the domain.

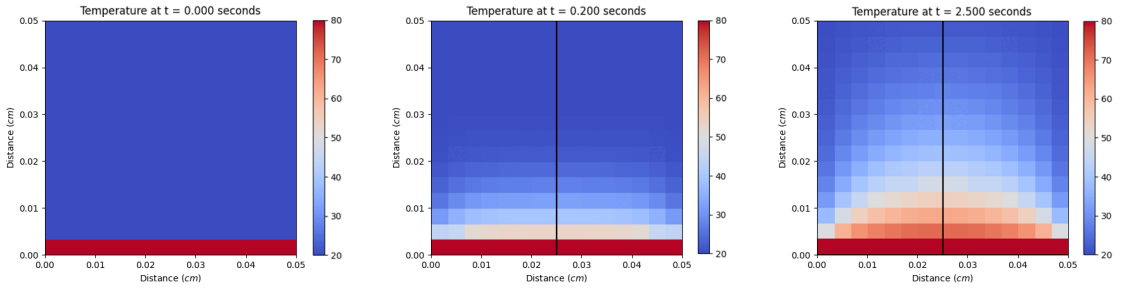

FIGURE 20: Heat distribution with a source at the bottom

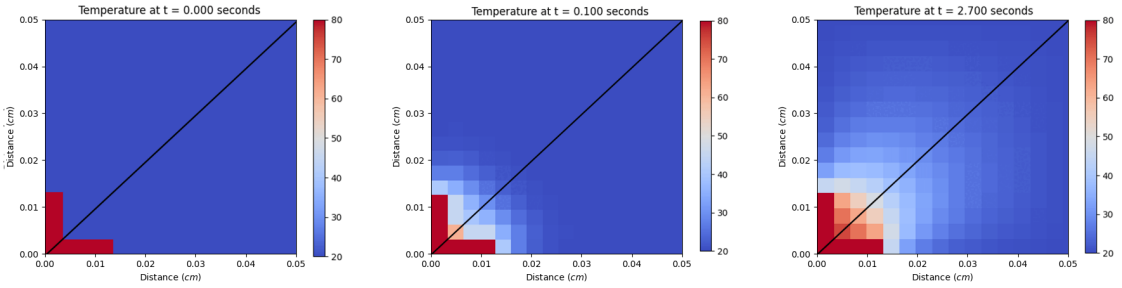

FIGURE 21: Heat distribution with source in the corner

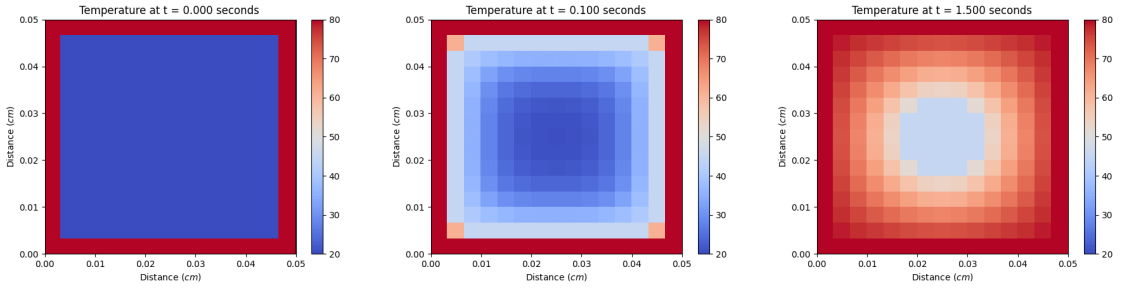

FIGURE 22: Heat distribution with source at the sides

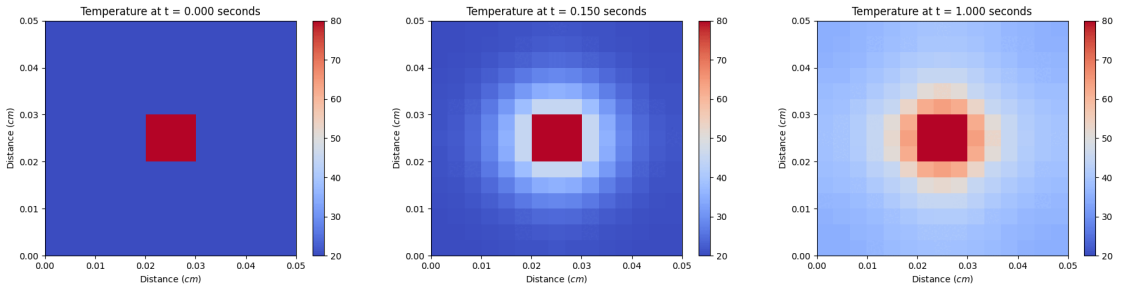

FIGURE 23: Heat distribution with source at the centre

The validation and verification that are conducted in this section indicate an accurate numerical implementation of two-phase Stefan problem for two-dimensional applications. This is supported by the validation of the one-dimensional scenario as demonstrated in Section 6.2. Furthermore, the geometric properties the heat distribution in both adiabatic and non-adiabatic systems contribute to the confirmation of the correctness of the implemented model.

In addition, we have validated that changing the parameters can result in an enhancement of the rate of the phase transition process. Utilizing this knowledge, we will now put our focus on examining the extent to which graphene nanofillers improve the performance of phase change materials.

6.4 Addition of graphene nanofillers

In the introduction of this study, a possible improvement of phase change materials was presented. This improvement relied on adding graphene nanofillers that should improve the overall conductivity of the phase change material, thereby improving the rate with which the heat spreads throughout the substance. In preceding sections, it was shown that this should indeed be the case, based on simulations and previous studies. In this section, we will investigate to which extent graphene nanofillers improve the heat distribution in phase change materials.

For convenience, we restate Table 3, which includes the chosen thermal properties for phase change materials with added graphene nanofillers.

TABLE 3: Parameters used for the simulation of the thermal behaviour of graphene

Symbol	Value	Unit
ρ	2000	kg m^{-3}
k	1	W $m^{-1}K^{-1}$
c_p	2	kJ $kg^{-1}K^{-1}$
L	150	kJ kg^{-1}

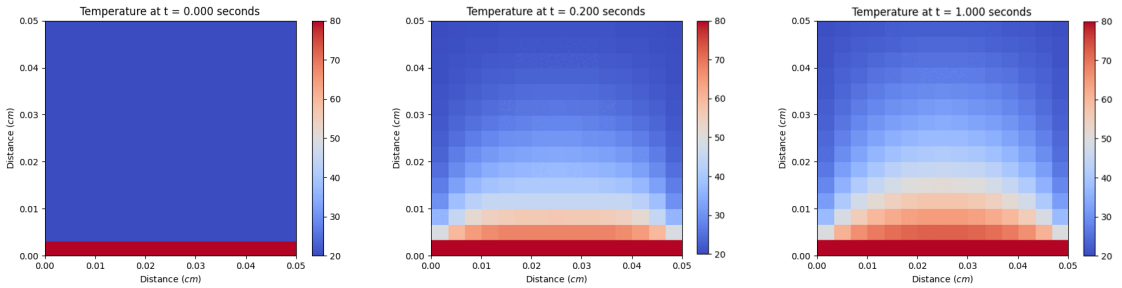

FIGURE 24: Heat distribution in paraffin wax with graphene nanofillers

In Figure 24, the heat dispersion in PCMs with graphene nanofillers can be observed. Note that this simulation has the same initial and non-adiabatic conditions as in Figure 20, hence the similarities. Upon closer inspection, we see can notice a difference between these figures. A comparison is given in Figure 25. We can see a significant increase in the spread of heat in the simulation with nanofillers. This implies that nanofillers indeed enhance the rate of which the phase transition process takes place. For this PCM, we used a conductivity of $k = 1$, which is an increase of 5 times the original value. In Figure 26, we present a case of more variations of the thermal conductivity in an adiabatic system, which may occur if a higher proportion of graphene is added to the mixture [21]. Again, we can see that the rate of the phase transition process is more noticeably more efficient with a higher thermal conductivity.

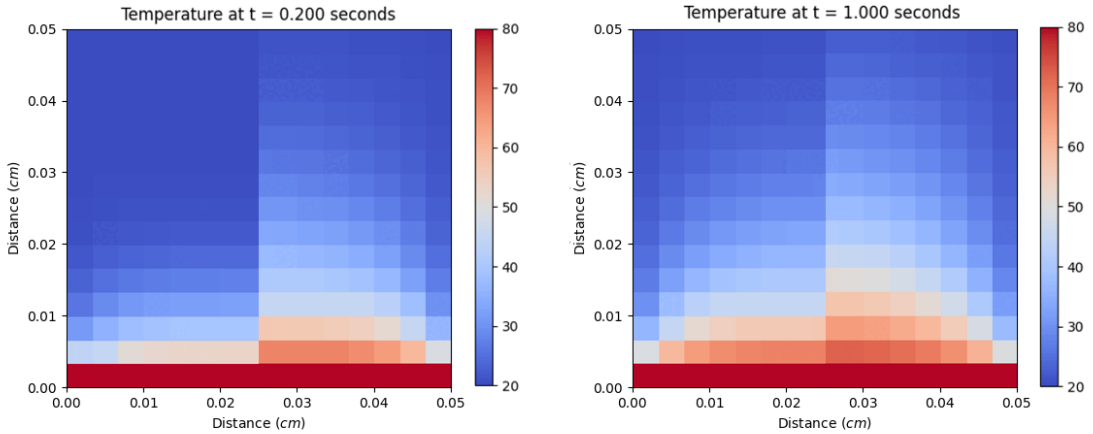

FIGURE 25: Side to side comparison of PCMs without (left) and with (right) graphene nanofillers in a non-adiabatic system

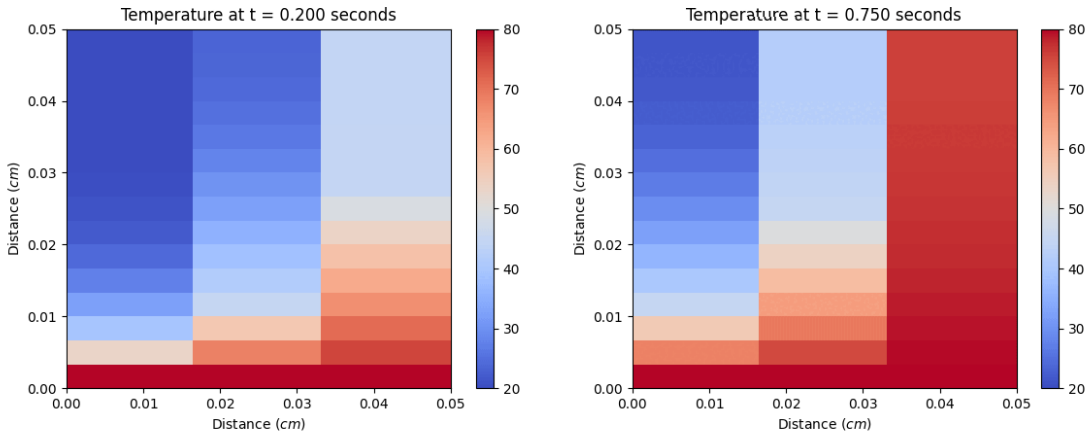

FIGURE 26: Side to side comparison of PCMs a conductivity of $k = 1, k = 2, k = 5$, respectively, in an adiatatic system

The conducted simulations provide valuable insights into the behaviour of phase change materials with the incorporation of graphene nanofillers. The numerical solutions obtained through the one- and two-dimensional simulations demonstrate the enhanced performance of PCMs during the solid-to-liquid phase transition if the nanofillers are added. These results validate the effect that graphene nanofillers have on the rate of the phase transition processes by improving the thermal characteristics of PCMs.

7 Discussion and recommendations

In this study, we investigated the Stefan problem and its application in the simulation of heat distribution. Specifically, we looked into the possible enhancement of phase change materials (PCMs) using graphene nanofillers. By obtaining its analytical and numerical solutions, we analyzed the impact of graphene nanofillers on the rate of the phase transition process.

Our analytical approach involved deriving expressions for the Stefan problem and Stefan condition, with which a one-dimensional solution was determined. Numerically, we utilized the enthalpy method to solve the Stefan condition. As was mentioned in Section 4, there are more methods that could have been used [15]. Future studies may consider investigating these methods, as they might yield more accurate approximations or might be computationally more advantageous.

We used the Forward Euler method to approximate the exact solution in both one- and multi-dimensional systems. The choice of the Forward Euler method was based on its simplicity and computational efficiency. However, the Forward Euler method has a drawback regarding the numerical stability and accuracy. Additionally, there was no clear convergence found in the convergence quotient Q. The reason of this inconsistency may be because of an incorrect implementation of the numerical method or because insufficiently small space and time steps were taken. To improve the accuracy and numerical stability, methods as Runge-Kutta or Crank-Nicolson may be considered for future studies. Hereby, the Runge-Kutta method increases the accuracy, whereas the Crank-Nicolson method improves the numerical stability. These techniques should yield a more precise representation of the exact solution of the phase transition process in PCMs.

Our findings indicated that the graphene nanofillers yield a noticeable improvement in the rate of the phase transition process by increasing the thermal diffusivity, which is in line with existing studies. In the simulations, parameters for the thermal properties were used. It is worth noting that the choice of parameters represented general values for a mixture of paraffin wax and graphene nanofillers, rather than a specific combination. Additionally, the mixture of graphene and paraffin is seen as a homogeneous substance, while in atomistic scale, this is not the case.

While our study focused specifically on graphene nanofillers, we have to consider that other nanofillers may yield varying effects on the thermal properties and thus on the rate of the phase transition process. Further research and experimentation should explore the potential of various nanofillers to enhance the performance of phase change material.

This study has underlined the potential of enhancing PCMs using appropriate nanofillers. By improving the numerical methods and conducting interdisciplinary research in collaboration with experts knowledgeable about thermal properties of PCMs, we may get a deeper understanding of PCMs. This research contributes to the development of more efficient and sustainable energy storage, ultimately contributing to a more sustainable world.

8 Conclusion

Our investigation into the Stefan problem and its application in simulations involving phase change materials (PCMs) has provided valuable insights into its thermal behaviour and performance enhancement by adding graphene nanofillers.
By exploring the incorporation of graphene nanofillers, we built upon existing studies that have shown a significant increase in thermal conductivity, while decreasing thermal properties as latent heat and specific heat capacity. Due to these changes, we found that the thermal diffusivity would increase accordingly. Consequently, our simulations showed an improvement in the rate of the phase transition processes in the cases where we added graphene nanofillers. These findings suggest the potential for graphene nanofillers to greatly enhance the performance of PCMs in applications such as thermal energy storage. Our study contributes to the growing understanding of the Stefan problem and its implications for PCMs. By leveraging the insights gained from this study, future research can further advance the development of efficient and sustainable thermal energy storage systems.

References

[1] Amir Reza Vakhshouri. "Paraffin as Phase Change Material". In: *Paraffin - an Overview*. IntechOpen, Dec. 2019. ISBN: 978-1-83880-595-1. DOI: 10.5772/intechopen.90487.

[2] Nihal Sarier and Emel Onder. "Organic phase change materials and their textile applications: An overview". In: *Thermochimica Acta* 540 (July 2012), pp. 7–60. DOI: 10.1016/j.tca.2012.04.013.

[3] Dawit Gudeta Gunjo et al. "Performance of latent heat storage (LHS) systems using pure paraffin wax as working substance". In: *Case Studies in Thermal Engineering* 39 (Nov. 2022). DOI: 10.1016/j.csite.2022.102399.

[4] Yajuan Zhong et al. "Heat transfer enhancement of paraffin wax using graphite foam for thermal energy storage". In: *Solar Energy Materials and Solar Cells* 94.6 (June 2010), pp. 1011–1014. DOI: 10.1016/j.solmat.2010.02.004.

[5] Mohamed Ashiq Ali et al. "Enhancement of heat transfer in paraffin wax PCM using nano graphene composite for industrial helmets". In: *Journal of Energy Storage* 26 (Dec. 2019). DOI: 10.1016/j.est.2019.100982.

[6] J. F. Li et al. "Simultaneous enhancement of latent heat and thermal conductivity of docosane-based phase change material in the presence of spongy graphene". In: *Solar Energy Materials and Solar Cells* 128 (Sept. 2014), pp. 48–51. DOI: 10.1016/j.solmat.2014.05.018.

[7] Jean Baptiste Joseph Fourier. *The Analytical Theory of Heat*. Trans. by Alexander Freeman. Cambridge Library Collection - Mathematics. Cambridge: Cambridge University Press, 2009. ISBN: 978-1-108-00178-6. DOI: 10.1017/CBO9780511693205.

[8] Richard Haberman. *Applied Partial Differential Equations with Fourier Series and Boundary Value Problems*. 5th. Pearson Education Limited, 2014.

[9] Daniele Andreucci. "Lecture notes on the Stefan problem". In: *Evolution equations and free boundary problems* (2004).

[10] Hahn David W. and Özışık M. Necati. "Phase-Change Problems". In: *Heat Conduction*. John Wiley & Sons, Ltd, 2012, pp. 452–495. ISBN: 978-1-118-41128-5. DOI: 10.1002/9781118411285.ch12.

[11] B N Antar, F G Collins, and A E Aumalis. "An Exact Solution for the Solidification of a Liquid Slab of Binary Mixture". In: *NASA Contractor Report 3962* (1986).

[12] Wonjoo Roh and Noboru Kikuchi. "Analysis of Stefan Problem with Level Set Method". In: *8th AIAA/ASME Joint Thermophysics and Heat Transfer Conference*. St. Louis, Missouri: American Institute of Aeronautics and Astronautics, June 2002. ISBN: 978-1-62410-118-2. DOI: 10.2514/6.2002-2874.

[13] Xu Quan-sheng et al. "Solution of the Two-Dimensional Stefan Problem by the Singularity-Separating Method". In: *Journal of Computational Mathematics* 3.1 (1985), pp. 8–18.

[14] S. Kutluay, A. R. Bahadir, and A. Özdeş. "The numerical solution of one-phase classical Stefan problem". In: *Journal of Computational and Applied Mathematics* 81.1 (June 1997), pp. 135–144. DOI: 10.1016/S0377-0427(97)00034-4.

[15] J. Caldwell and Y. Y. Kwan. "Numerical methods for one-dimensional Stefan problems". In: *Communications in Numerical Methods in Engineering* 20.7 (2004), pp. 535–545. DOI: 10.1002/cnm.691.

[16] Sri Redjeki Pudjaprasetya. *Transport Phenomena, equations and numerical methods*. July 2018. DOI: 10.31227/osf.io/5vw73.

[17] R. E. White. "An Enthalpy Formulation of the Stefan Problem". In: *SIAM Journal on Numerical Analysis* 19.6 (1982), pp. 1129–1157.

[18] Dede Tarwidi. "An enthalpy-based finite element method for solving two-phase Stefan problem". In: *Indonesian Journal on Computing (Indo-JC)* 4 (Mar. 2019), p. 43. DOI: 10.21108/INDOJC.2019.4.1.252.

[19] *DiracDelta Science & Engineering Encyclopedia*. Specific Heat Capacity. Aug. 2007.

[20] Miqdam Chaichan, Shaimaa Hilal Kamel, and Al-Ajeely M. "Thermal Conductivity Enhancement by using Nano-material in Phase Change Material for Latent Heat Thermal Energy Storage Systems". In: *SAUSSUREA* 5 (Aug. 2015), pp. 48–55.

[21] Hengxing Ji et al. "Enhanced thermal conductivity of phase change materials with ultrathin-graphite foams for thermal energy storage". In: *Energy & Environmental Science* 7.3 (Feb. 2014), pp. 1185–1192. DOI: 10.1039/C3EE42573H.